Transcriptional coactivator Cited2 induces Bmi1 and Mel18 and controls fibroblast proliferation via Ink4a/ARF

MOLECULAR AND CELLULAR BIOLOGY, Nov. 2003, p. 7658–7666 Vol. 23, No. 21
0270-7306/03/$08.00+0 DOI: 10.1128/MCB.23.21.7658–7666.2003

Transcriptional Coactivator Cited2 Induces Bmi1 and Mel18 and Controls Fibroblast Proliferation via *Ink4a/ARF*

Kamil R. Kranc,[1,2] Simon D. Bamforth,[1] José Bragança,[1] Chris Norbury,[3] Maarten van Lohuizen,[4] and Shoumo Bhattacharya[1]*

Departments of Cardiovascular Medicine[1] and Biochemistry,[2] Wellcome Trust Centre for Human Genetics, and Sir William Dunn School of Pathology,[3] University of Oxford, Oxford, United Kingdom, and Division of Molecular Genetics, The Netherlands Cancer Institute, Amsterdam, The Netherlands[4]

Received 10 April 2003/Returned for modification 19 May 2003/Accepted 14 July 2003

***Cited2* (CBP/p300 interacting transactivator with ED-rich tail 2) is required for embryonic development, coactivation of transcription factor AP-2, and inhibition of hypoxia-inducible factor 1 transactivation. *Cited2* is induced by multiple growth factors and cytokines and oncogenically transforms cells. Here, we show that the proliferation of *Cited2*$^{-/-}$ mouse embryonic fibroblasts ceases prematurely. This is associated with a reduction in growth fraction, senescent cellular morphology, and increased expression of the cell proliferation inhibitors p16^{INK4a}, p19^{ARF}, and p15^{INK4b}. Deletion of *INK4a/ARF* (encoding p16^{INK4a} and p19^{ARF}) completely rescued the defective proliferation of Cited2$^{-/-}$ fibroblasts. However, the deletion of *INK4a/ARF* did not rescue the embryonic malformations observed in *Cited2*$^{-/-}$ mice, indicating that *INK4a/ARF*-independent pathways are likely to be involved here. We found that *Cited2*$^{-/-}$ fibroblasts had reduced expression of the polycomb-group genes *Bmi1* and *Mel18*, which function as *INK4a/ARF* and *Hox* repressors. Complementation with CITED2-expressing retrovirus enhanced proliferation, induced *Bmi1/Mel18* expression, and decreased *INK4a/ARF* expression. Bmi1- and Mel18-expressing retroviruses enhanced the proliferation of *Cited2*$^{-/-}$ fibroblasts, indicating that they function downstream of *Cited2*. Our results provide genetic evidence that *Cited2* controls the expression of *INK4a/ARF* and fibroblast proliferation, at least in part via the polycomb-group genes *Bmi1* and *Mel18*.**

p300 and its paralog, CBP (CREB-binding protein), are ubiquitously expressed nuclear proteins that function as transcriptional coactivators and histone acetyl transferases, connecting DNA-bound transcription factors to the core transcriptional machinery (reviewed in references 19 and 50). p300 and CBP are essential for normal cardiovascular, neural, and hematopoietic development (31, 39, 60). p300 and CBP also play a fundamental role in cellular growth control (reviewed in reference 19). Genetic evidence indicates that CBP is a tumor suppressor. Patients with CBP mutations (Rubinstein-Taybi syndrome) (41) have a high incidence of neural and developmental tumors (38), and mice lacking a single CBP allele develop hematological malignancies (31). Consistent with this finding, p300 and CBP function as coactivators of the tumor suppressor p53 (8, 34). Paradoxically, p300 and CBP are also required for cell proliferation. Embryonic fibroblasts lacking p300 proliferate poorly in culture (60), and neutralization of p300/CBP by antibody injection inhibits progression through the G_1/S transition (1). In keeping with this finding, many oncogenic transcription factors require either p300 or CBP for transactivation (reviewed in reference 19).

p300 and CBP also interact with members of the CBP/p300 interacting transactivator with ED-rich tail (CITED) family. These include CITED1/MSG1 (58); CITED2, splice isoforms of which are known as p35srj/Mrg1 (12, 33); and CITED4 (15, 59). Loss of *Cited2* in mice results in embryonic lethality as a consequence of cardiac malformations, neural tube defects, and adrenal gland agenesis (9, 10, 43, 57, 61). At a biochemical level, CITED2 physically interacts with and coactivates all transcription factor AP-2 (TFAP2) isoforms and is necessary for TFAP2 function (9, 14). CITED2 also inhibits hypoxia-inducible factor 1 alpha (HIF-1α) transactivation by disrupting the HIF-1α–p300 interaction (12, 61). These molecular mechanisms are thought to underlie the embryonic malformations observed in mice lacking *Cited2*. CITED2 is induced by multiple growth factors and cytokines (e.g., interleukin-1α [IL-1α], IL-2, IL-4, IL-6, IL-9, IL-11, granulocyte-macrophage colony-stimulating factor, platelet-derived growth factor, and insulin), and overexpression of CITED2 results in oncogenic cell transformation (51). The response of CITED2 to mitogenic stimuli and its ability to transform cells suggest that it may function in cell growth control (51). To understand the genetic pathways by which CITED2 may control cell proliferation, we studied mouse embryonic fibroblasts lacking *Cited2*.

MATERIALS AND METHODS

Mice. *Cited2*$^{-/-}$ and *Cited2*$^{+/+}$ embryos were on a 129Ola/C57BL/6J mixed background or a C57BL/6J background as indicated and were generated as previously described (9). *Cited2*$^{-/-}$*:INK4a/ARF*$^{-/-}$ (INK4, inhibitor of cyclin-dependent kinase; ARF, alternative reading frame) embryos and the relevant controls (see Fig. 5 and 6) were on an FVB/129Ola/C57BL/6J mixed background and were generated by intercrossing *Cited2*$^{+/-}$*:INK4a/ARF*$^{+/-}$ mice. *INK4a/ARF*$^{+/-}$ mice (45) were kind gifts from Ronald DePinho (DFCI, Boston, Mass.). Mice, embryos, and fibroblasts were genotyped by using PCR with allele-specific primers (9).

* Corresponding author. Mailing address: Department of Cardiovascular Medicine, University of Oxford, Wellcome Trust Centre for Human Genetics, Roosevelt Drive, Oxford OX3 7BN, United Kingdom. Phone: 44-1865-287581. Fax: 44-1865-287661. E-mail: sbhattac@well.ox.ac.uk.

Fibroblast isolation, passage, growth curves, and colony formation assays. Murine embryonic fibroblasts were prepared from littermate embryos at 13.5 or 15.5 days postcoitum (dpc) as previously described (36). Adherent fibroblasts were harvested the following day and plated at a density of 1.5×10^4 cells per cm^2 (passage 0) and passaged every 3 days thereafter at the same density. Population doubling per passage was calculated as $\log(n_f/n_o)/\log 2$, where n_o is the initial and n_f the final number of cells at each passage (13). When n_o was greater than n_f, the population doubling was defined as 0. Cumulative population doubling (CPD) at each passage was calculated by adding population doubling per passage (13). Senescence-associated β-galactosidase was detected as previously described (17). For growth curves, the indicated number of cells per well of a 12-well plate were plated and harvested at the indicated time points and relative cell numbers were measured with crystal violet as previously described (46). Values were normalized to day 1 for the indicated culture, and each point was determined in quadruplicate. For colony formation, fibroblasts were plated at the densities indicated and the colonies were visualized with Giemsa stain as previously described (13).

Growth fraction. Cells were plated at a density of $1.5 \times 10^4/cm^2$ onto glass coverslips at the indicated passages, and after 48 h, 10 μM bromodeoxyuridine (BrdU) was added for 24 h. The coverslips were fixed, incubated in HCl, and then stained with anti-BrdU monoclonal antibody (Becton-Dickinson) followed by secondary sheep anti-mouse fluorescein isothiocyanate-conjugated antibody. Cells were stained with propidium iodide (PI) and mounted in Vectashield containing PI (Vector). Nuclear uptake of BrdU and PI was quantitated on a laser scanning cytometer (CompuCyte, Cambridge, Mass.) and analyzed with WinCyte software according to the manufacturer's instructions. Data from the results for 3,000 to 5,000 cells were acquired for each individual experiment. The growth fraction was calculated as the percentage of BrdU-positive cells in the culture.

Retroviruses. CITED2, CITED2Δ, Mel18, Bmi1, and control retroviral supernatants were generated by using the bicistronic pLZRS-IRES-GFP plasmid and Phoenix producer cells (gifts from Garry Nolan, Stanford, Calif.). Fibroblasts were infected as previously described (25). The *Bmi1* retrovirus has been described previously (25). The *Mel18* retrovirus was generated from pSG5-Mel18, which contains a mouse Mel18 cDNA insert (gift from M. Kanno, Hiroshima, Japan) with a modified translation start site (GCCACCATGG) that changes the second amino acid from H to D. We used PCR to convert the Mel18 translation start site back to the wild-type form (GGCATCATGC) (GenBank accession no. D90085) and subcloned an *Eco*RI-*San*DI fragment (containing the open reading frame) into pLZRS-IRES-GFP. Infection efficiencies typically exceeded 80%. Plasmid vectors were generated by using standard molecular cloning techniques (7).

Blotting. Northern blotting was performed as previously described (7) by using 6 to 10 μg of total RNA (RNeasy Mini-kit, QIAGEN) transferred to Hybond N+ membranes (Amersham). 28S and 18S rRNA species were visualized by staining with 0.05% methylene blue. Murine $p19^{ARF}$, $p19^{INK4d}$, and $p15^{INK4b}$ cDNA plasmids were gifts from Charles Sherr (HHMI, Memphis, Tenn.) and Gordon Peters (Cancer Research UK, London, United Kingdom). $p16^{INK4a}$- and $p19^{ARF}$-specific probes (*INK4a/ARF1*α and *INK4a/ARF1*β) were generated from respective cDNA templates by PCR by using exon-specific primers. Northern blotting for Mel18, Bmi1, and Mph1 was performed from early passage, nonconfluent mouse embryonic fibroblasts by using the respective murine probes. The Mph1 probe (IMAGE:3512187) was obtained from MRC-HGMP, Cambridge, United Kingdom. The relative signal intensity was measured by using NIH Image software on scanned autoradiograms. Western blotting with anti-Bmi1 monoclonal antibody (229F6; Upstate Biotechnology, Lake Placid, N.Y.), $p16^{INK4a}$ (M156; Santa Cruz) and anti-$p19^{ARF}$ (Ab80; Abcam, Cambridge, United Kingdom) polyclonal antibodies, and antitubulin antibody (T-5293; Sigma) was performed according to the instructions of the manufacturer.

Histology. Embryos were fixed in 4% paraformaldehyde, dehydrated in ethanol, and embedded in paraffin wax. Sections (7 μm thick) were stained with hematoxylin and eosin.

RESULTS

Premature proliferation arrest of *Cited2*$^{-/-}$ fibroblasts. We investigated the proliferative capacity of *Cited2*$^{+/+}$ and *Cited2*$^{-/-}$ primary mouse embryonic fibroblasts. Fibroblasts were derived from littermate embryos and passaged every 3 days in parallel and under identical conditions at a density of 1.5×10^4 cells/cm^2, equivalent to a 3T3 protocol (36). *Cited2*$^{+/+}$ fibroblasts proliferated rapidly and then slowed transiently at passages 5 and 6, following which proliferation was rapid and continuous (Fig. 1A). *Cited2*$^{-/-}$ fibroblasts proliferated normally in the first three passages but slowed dramatically and then arrested permanently. This premature proliferation arrest was confirmed in three independent experiments by using independently isolated fibroblasts (data not shown) as well as fibroblasts isolated from coisogenic mice generated by backcrossing the *Cited2* mutation to the C57BL/6J background for more than nine generations (Fig. 1B). These results were also corroborated by plating fibroblasts at passage 3 and assaying cell growth over the next 14 days without replating (Fig. 1C). By passage 3, the *Cited2*$^{-/-}$ fibroblasts had a decreased ability to proliferate in comparison to that of the *Cited2*$^{+/+}$ fibroblasts. Cultures of either genotype had indistinguishable spindle-shaped cells at initial plating. With passage, *Cited2*$^{-/-}$ fibroblast cultures rapidly accumulated cells that had a flattened appearance and cytoplasmic enlargement and expressed senescence-associated β-galactosidase (17) (Fig. 1D and E).

Reduction in growth fraction. To determine the mechanism of impaired proliferation in *Cited2*$^{-/-}$ fibroblasts, the fraction of actively proliferating cells (11) was measured by labeling parallel cultures with BrdU for 24 h. Bivariate analysis for BrdU uptake and PI staining showed that the growth fraction of *Cited2*$^{+/+}$ and *Cited2*$^{-/-}$ fibroblasts was close to 100% when initially placed in culture (Fig. 2A and B). With serial passage, the growth fraction of *Cited2*$^{-/-}$ fibroblasts declined more rapidly than that of *Cited2*$^{+/+}$ fibroblasts. The fall in growth fraction in the *Cited2*$^{-/-}$ cultures was evident as early as the first passage. All cultures were initially predominantly diploid, as determined by PI staining (Fig. 2A). With serial passage, cultures became tetraploid (Fig. 2A, middle and lower panels). Although the wild-type culture shown in the top panel of Fig. 2A was still predominantly diploid at this passage, it became predominantly tetraploid at the next passage (data not shown).

***Cited2*$^{-/-}$ fibroblasts have increased expression of *INK4a/ARF*.** The above results showed that *Cited2*$^{-/-}$ fibroblasts cease to proliferate prematurely when cultured, do not spontaneously immortalize, and express morphological features of cellular senescence. Senescence in mouse embryonic fibroblasts is associated with increased levels of the alternatively spliced products of the *INK4a/ARF* locus, $p16^{INK4a}$, and $p19^{ARF}$ (Fig. 3A) (reviewed in references 48 and 49). Members of the INK4 family function to inhibit cyclin-dependent kinases 4 and 6, whereas $p19^{ARF}$ functions to inhibit MDM2, a repressor of p53. We examined the expression of *INK4a/ARF* in early passage *Cited2*$^{+/+}$ and *Cited2*$^{-/-}$ fibroblasts (Fig. 3B through F). Northern blots were probed with a $p19^{ARF}$ cDNA, which detects both $p16^{INK4a}$ and $p19^{ARF}$ (Fig. 3A and B) as comigrating products. This probe showed that *INK4a/ARF* expression was clearly increased (2.7-fold) in *Cited2*$^{-/-}$ fibroblasts (Fig. 3B). Specific probes that discriminate between the alternatively spliced $p16^{INK4a}$ and $p19^{ARF}$ transcripts showed that the expression of both transcripts was increased (4.2- and 2.7-fold, respectively) in fibroblasts lacking *Cited2* (Fig. 3C and D). The expression of $p15^{INK4b}$, a member of the INK4 family (21) (Fig. 3E), was also increased (2.5-fold) in *Cited2*$^{-/-}$ fibroblasts (Fig. 3A). We observed no change in the expression of $p19^{INK4d}$, another INK4 family member (23) (Fig. 3F). Consistent with these observations, the levels of $p16^{INK4a}$ and

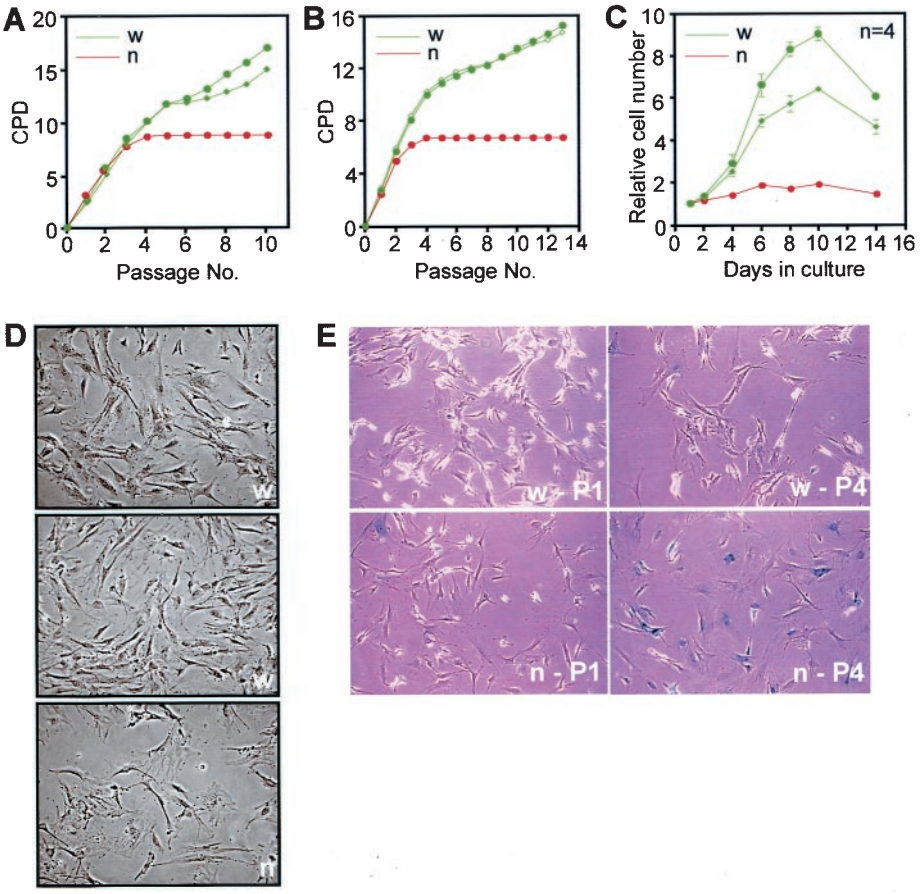

FIG. 1. Proliferation properties and morphology of *Cited2*$^{-/-}$ mouse embryonic fibroblasts. (A) Cumulative growth of *Cited2*$^{+/+}$ (w) and *Cited2*$^{-/-}$ (n) fibroblast cultures prepared from 15.5-dpc embryos on a 129Ola/C57BL/6J mixed background shown as a plot of CPD versus passage number. (B) These results are also reproduced in *Cited2*$^{+/+}$ (w) and *Cited2*$^{-/-}$ (n) fibroblast cultures isolated from 13.5-dpc embryos on a coisogenic C57BL/6J background. (C) Proliferative capacity of fibroblasts at passage 3. Fibroblasts prepared from embryos on a 129Ola/C57BL/6J background were plated in quadruplicate into 12-well plates (6×10^3 cells per well) and fixed at the indicated time points, and relative cell numbers were determined by using crystal violet. Data (means ± standard errors of the means [SEMs]) were normalized for cell numbers at day 1. (D) Morphology of *Cited2*$^{+/+}$ (w) and *Cited2*$^{-/-}$ (n) fibroblasts at passage 4. *Cited2*$^{-/-}$ cultures rapidly accumulate cells that appear flat with cytoplasmic enlargement. (E) *Cited2*$^{+/+}$ (w) and *Cited2*$^{-/-}$ (n) fibroblasts were stained for senescence-associated β-galactosidase at passage 1 (P1) or passage 4 (P4).

p19^{ARF} proteins were also increased (2.5- and 2.7-fold, respectively) in *Cited2*$^{-/-}$ fibroblasts at passage 1 (Fig. 3G and H).

Complementation with CITED2 enhances proliferation. To determine if these changes were specific for loss of *Cited2*, we infected *Cited2*$^{-/-}$ fibroblasts with a bicistronic retrovirus expressing human CITED2 (which is 94% conserved with mouse Cited2) and GFP (green fluorescent protein) driven by a retroviral long terminal repeat (Fig. 4A). These fibroblasts showed a marked enhancement of proliferation that was maintained for the period studied (i.e., greater than 30 days) and retained their spindle shape (data not shown). In comparison, parallel infection with a control GFP-expressing retrovirus (LZRS) or with retrovirus expressing CITED2Δ, a mutant lacking the overlapping CBP/p300 and TFAP2 binding domains (9, 12), did not enhance proliferation. These results were confirmed in two further experiments using independently isolated *Cited2*$^{-/-}$ fibroblasts. Infection of *Cited2*$^{-/-}$ fibroblasts with the CITED2-expressing retrovirus also led to a modest reduction in *INK4a/ARF* and *INK4b* expression (1.5- and 1.6-fold, respectively) (Fig. 4B and C) in comparison to control retrovirus.

An intact *INK4a/ARF* gene is essential for proliferation arrest in *Cited2*$^{-/-}$ fibroblasts. The above results suggested that *Cited2* enhances fibroblast proliferation by repressing *INK4a/ARF* and/or *INK4b*. To definitively establish the role of *INK4a/ARF* in mediating the premature proliferation arrest of *Cited2*$^{-/-}$ fibroblasts, we generated fibroblasts lacking both *Cited2* and *INK4a/ARF* (*Cited2*$^{-/-}$:*INK4a/ARF* $^{-/-}$) and compared their proliferation with that of *Cited2*$^{-/-}$:*INK4a/ARF*$^{+/+}$, *Cited2*$^{+/+}$:*INK4a/ARF*$^{-/-}$, and wild-type fibroblasts (Fig. 5A and B). Consistent with previous observations (45), fibroblasts lacking *INK4a/ARF* proliferated more rapidly than wild-type fibroblasts during serial passage in culture, with no slowing of proliferation for the duration of the experiment (48 days). Consistent with the observations in Fig. 1, *Cited2*$^{-/-}$ fibroblasts arrested prematurely and permanently. Fibroblasts lacking both *Cited2* and *INK4a/ARF* proliferated almost as rapidly as those lacking *INK4a/ARF*, with no slowing of prolif-

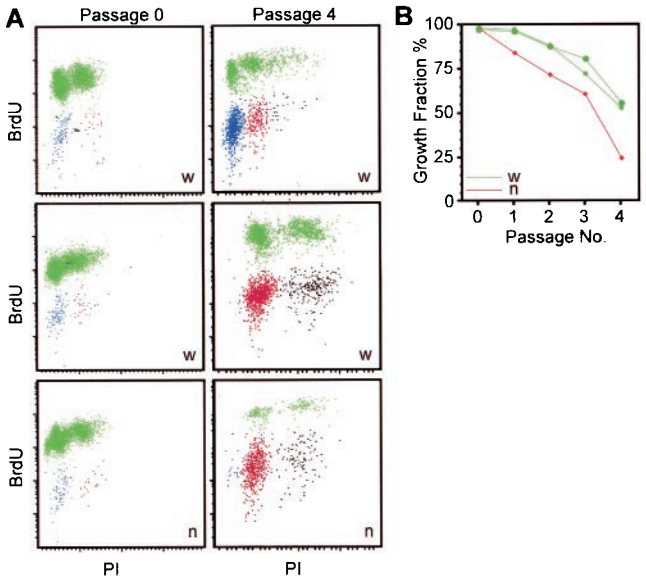

FIG. 2. Growth fraction of *Cited2*$^{-/-}$ mouse embryonic fibroblasts. (A) Scattergrams of nuclear DNA synthesis (BrdU) vs. DNA content (PI) of *Cited2*$^{+/+}$ (w) and *Cited2*$^{-/-}$ (n) fibroblast cultures at passages 0 and 4. BrdU-labeled cells are indicated in green. Unlabeled cells are indicated in blue (2n), red (4n), or black (8n DNA content). (B) Growth fraction of *Cited2*$^{-/-}$ and *Cited2*$^{+/+}$ fibroblast cultures plotted against passage number.

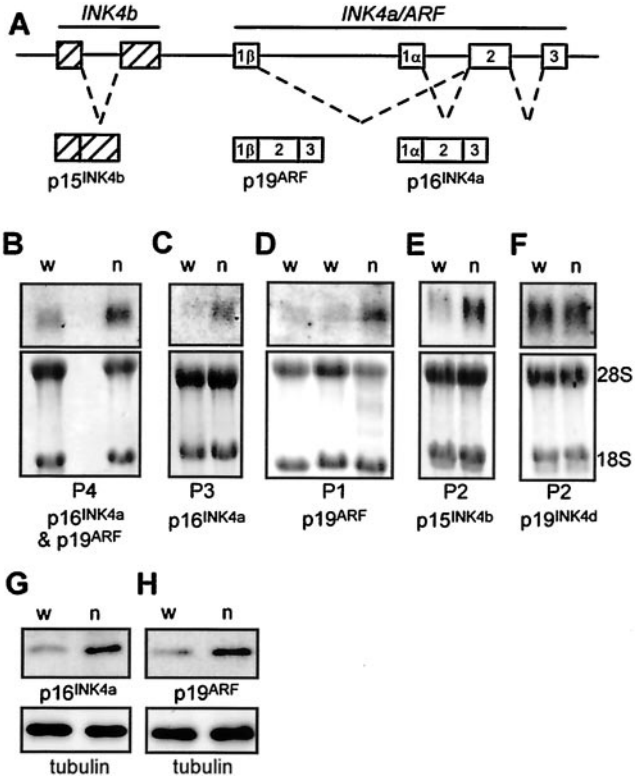

FIG. 3. *INK4a/ARF* expression in *Cited2*$^{-/-}$ fibroblasts. (A) Representation of the *INK4a/ARF* and *INK4b* locus showing exon structure and alternative splicing (dashed lines) that generates the three different cell cycle inhibitors p15^{INK4b}, p16^{INK4a}, and p19^{ARF}. (B through F) Northern blots of total RNA obtained from independent pairs of *Cited2*$^{+/+}$ (w) and *Cited2*$^{-/-}$ (n) fibroblasts derived from littermate embryos. The passage number (P) is indicated in each panel. (B) A full-length p19^{ARF} cDNA was used as a probe. This probe detects both p19^{ARF} and p16^{INK4a} isoforms, which comigrate. (C) p16^{INK4a} was detected by using a specific exon 1α probe. (D) p19^{ARF} was detected by using a specific exon 1β probe. (E and F) p15^{INK4b} and p19^{INK4d} transcripts were detected by using full-length cDNA probes. The bottom section in each panel shows 28S and 18S RNA species, confirming equal loading. (G and H) Western blots of total cell lysates from *Cited2*$^{+/+}$ and *Cited2*$^{-/-}$ fibroblasts at passage 1 were probed with anti-p16^{INK4a} and anti-p19^{ARF} antibodies (top panels) and with an antitubulin monoclonal antibody (bottom panels) to demonstrate equal loading.

eration. These results were further confirmed in independently isolated fibroblasts lacking both *Cited2* and *INK4a/ARF* (data not shown). We then examined the proliferative capacity of these fibroblasts by plating them at passage 4 and assaying cell growth over the next 10 days without replating (Fig. 5C). In keeping with the above observations, *Cited2*$^{-/-}$ fibroblasts had markedly reduced proliferative ability, and *INK4a/ARF*$^{-/-}$ fibroblasts proliferated more rapidly than wild-type fibroblasts. Fibroblasts lacking both *Cited2* and *INK4a/ARF* proliferated as rapidly as those lacking only *INK4a/ARF*. We also examined the ability of these fibroblasts to form colonies when plated at low density, an independent measure of the proliferative potential of primary cells (13). In this assay, wild-type and *Cited2*$^{-/-}$ fibroblasts formed small colonies with very low efficiency (Fig. 5D). *INK4a/ARF*$^{-/-}$ fibroblasts efficiently formed large colonies. Fibroblasts lacking both *Cited2* and *INK4a/ARF* formed colonies almost as well as those lacking only *INK4a/ARF*. These results indicate that intact *INK4a/ARF* function is essential for the reduced proliferative capacity and premature proliferation arrest observed in *Cited2*$^{-/-}$ fibroblasts.

Elimination of *INK4a/ARF* does not rescue embryonic malformations in *Cited2*$^{-/-}$ mice. To determine if *INK4a/ARF* plays a role in the genesis of embryonic malformations in mice lacking *Cited2*, we examined embryos lacking both *Cited2* and *INK4a/ARF*. Like embryos lacking only *Cited2* (9), those lacking both *Cited2* and *INK4a/ARF* had cardiac malformations (Fig. 6B), adrenal agenesis (Fig. 6D), and exencephaly (Fig. 6F). In these experiments, exencephaly was observed in 4 of 8 embryos lacking *Cited2* and 6 of 13 embryos lacking both *Cited2* and *INK4a/ARF*. Control embryos that were wild type for *Cited2* but lacked *INK4a/ARF* had normal heart, adrenal, and neural development (Fig. 6A, C, and E). These results indicate that *Cited2* controls other pathways that are relevant for embryonic development.

Cells lacking *Cited2* have reduced Bmi1 and Mel18 expression. The above data indicated that *Cited2* enhances cell proliferation by repressing *INK4a/ARF*. Genetic evidence indicates that in primary mouse fibroblasts the polycomb-group gene *Bmi1* represses p16^{INK4a} and p19^{ARF} and that *Mel18* (a *Bmi1* paralog) represses p16^{INK4a} (25). We therefore examined the expression of these genes in early passage *Cited2*$^{+/+}$ and *Cited2*$^{-/-}$ fibroblasts derived from littermate embryos. We found that both Mel18 and Bmi1 expression was reduced (2.3- and 2.2-fold, respectively) in *Cited2*$^{-/-}$ fibroblasts (Fig. 7A and B). There was no significant change in the expression of *Mph1*, another polycomb group gene. We also examined the fibroblasts for *TBX2*, another *INK4a/ARF* repressor (24), but expression of this gene was not detected in wild-type or *Cit-*

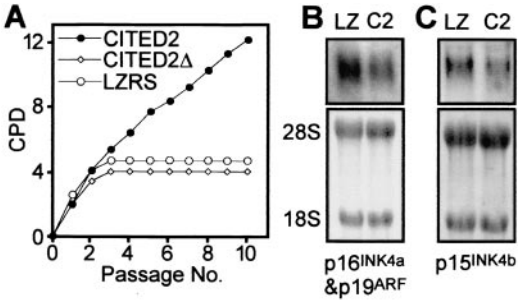

FIG. 4. Complementation of *Cited2*$^{-/-}$ fibroblasts with CITED2. (A) *Cited2*$^{-/-}$ fibroblasts (derived from an embryo at 13.5 dpc) were infected with CITED2, CITED2Δ (lacking residues 215 to 270), or LZRS (control) retrovirus. Infected fibroblasts were replated on day 7 (passage 0) and passaged every 3 days. Cumulative growth of retrovirally complemented *Cited2*$^{-/-}$ fibroblasts is shown as a plot of CPD versus passage number. The results were reproduced in two further independent experiments by using independently isolated fibroblasts. (B and C) Northern blots of total RNA obtained from retrovirally complemented *Cited2*$^{-/-}$ fibroblasts. LZ indicates infection with LZRS (control) retrovirus, and C2 indicates infection with CITED2-expressing retrovirus. The transcripts detected are indicated in each panel. The bottom panels in each figure show 28S and 18S RNA species, confirming equal loading. (B) A full-length p19^{ARF} cDNA was used as a probe. This probe detects both p19^{ARF} and p16^{INK4a} isoforms, which comigrate. (C) A p15^{INK4b} transcript was detected by using a full-length cDNA probe.

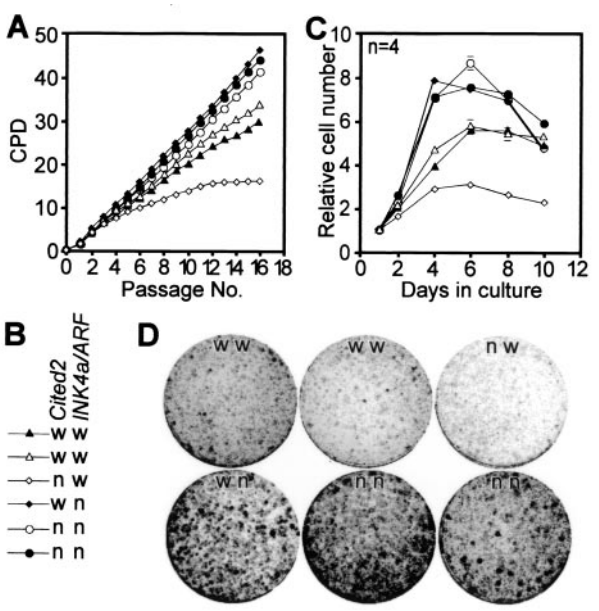

FIG. 5. Proliferative properties of fibroblasts lacking both *Cited2* and *INK4a/ARF*. (A and B) Fibroblasts were harvested simultaneously from independent embryos at 13.5 dpc. Cumulative fibroblast growth is shown as a plot of CPD versus passage number. Each line represents fibroblasts isolated from an independent embryo. Fibroblast genotypes (w, wild-type; n, null) for *Cited2* and *INK4a/ARF* alleles are indicated in panel B. (C) Proliferative capacity of fibroblasts at passage 4. Fibroblasts were plated in quadruplicate into 12-well plates (2.5×10^4 cells per well) and fixed at the indicated time points, and relative cell numbers were determined by using crystal violet as previously described (25). Data (means ± SEMs) were normalized for cell numbers at day 1. The genotypes are indicated in panel B. (D) Colony formation assay. Fibroblasts (passage 1) were plated at a density of 4,000 cells per 9-cm plate, and colonies were visualized with Giemsa stain after 7 days. Fibroblast genotypes are indicated as wild-type (w) or null (n) for *Cited2* and *INK4a/ARF* alleles, as indicated in panel B.

ed2$^{-/-}$ fibroblasts (data not shown). Infection of *Cited2*$^{-/-}$ fibroblasts with CITED2-expressing retrovirus resulted in a modest increase in expression of Mel18 (1.5-fold) and Bmi1 (1.4-fold) (Fig. 7C and D).

Bmi1 and Mel18 enhance proliferation of cells lacking *Cited2*. The above data indicated that *Cited2* is required for normal Bmi1 and Mel18 expression. To determine if the observed deficiency of Bmi1 and Mel18 expression in *Cited2*$^{-/-}$ fibroblasts would explain their premature proliferation arrest, we infected *Cited2*$^{-/-}$ and *Cited2*$^{+/+}$ fibroblasts with bicistronic retroviruses expressing either Bmi1 and GFP, Mel18 and GFP, or GFP alone (as the control) and performed cell proliferation and colony formation assays (Fig. 8A and B). Infection with Bmi1- or Mel18-expressing retroviruses led to enhanced proliferation compared to that for the control retrovirus, regardless of the *Cited2* genotype (Fig. 8A). The Bmi1 retrovirus enhanced proliferation better than the Mel18 retrovirus, again regardless of *Cited2* genotype. We next examined the ability of these fibroblasts to form colonies when plated at low density (Fig. 8B). Consistent with the above results, infection with Bmi1- or Mel18-expressing retroviruses led to enhanced colony formation (with Bmi1 being more efficient than Mel18) compared to that for the control retrovirus, regardless of the *Cited2* genotype. This enhancement of proliferation by Bmi1 and by Mel18 was reproducibly observed in *Cited2*$^{-/-}$ fibroblasts obtained from independently harvested embryos. These results indicate that Bmi1 or Mel18 can enhance the proliferation of fibroblasts lacking *Cited2* and that *Cited2* function is not required for proliferation enhancement by these polycomb-group proteins.

DISCUSSION

Normal primary mouse embryonic fibroblasts proliferate rapidly when explanted but soon slow down in response to the stress of culture (reviewed in reference 48). This is associated with cell cycle exit, cytoplasmic enlargement, and expression of senescence-associated β-galactosidase, which are characteristics of cellular senescence (17). At a molecular level in murine cells, this senescent phenotype is associated with increased levels of the cell proliferation inhibitors p16^{INK4a} and p19^{ARF} and activation of the p19^{ARF} target p53 and the p53 target gene *p21*^{CIP1} (reviewed in references 48 and 49). Genetic evidence indicates that intact *p19*^{ARF} and *p53* are necessary for the senescent phenotype of cultured mouse embryonic fibroblasts (45; reviewed in reference 48). Deletion of *p19*^{ARF} alone abolishes the senescent phenotype, whereas deletion of *p16*^{INK4a} alone does not have this effect, indicating that *p19*^{ARF} plays a critical role (28, 30, 47). Notably, the spontaneous immortalization of wild-type fibroblasts observed when they are serially passaged in culture typically results from spontaneous mutations in *p19*^{ARF} or *p53* (28, 62). Premature senescence of primary fibroblasts is associated with mutations in genes such as *Bmi1*, *JunD*, *Atm*, and *Lig4* that function upstream of p19^{ARF} (18, 25, 27, 56). It is also associated with mutations in *Mel18* (25) and *Id1* (5), which repress p16^{INK4a} expression. Overexpression of activated cellular oncogenes

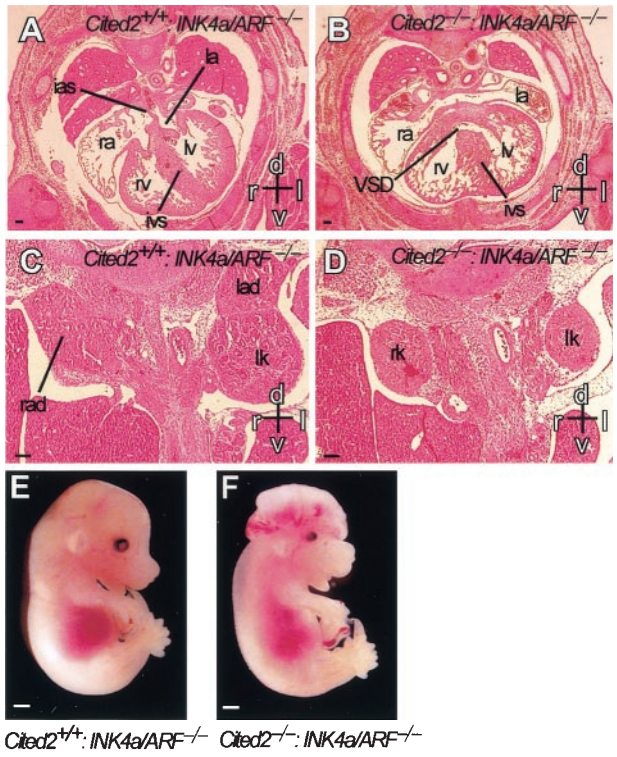

FIG. 6. Embryonic malformations in embryos lacking both *Cited2* and *INK4a/ARF*. (A through D) Hematoxylin- and eosin-stained transverse sections from *Cited2*$^{+/+}$:*INK4a/ARF*$^{-/-}$ and *Cited2*$^{-/-}$:*INK4a/ARF*$^{-/-}$ embryos at 14.5 dpc. Scale bars, 0.1 mm. Axes: d, dorsal; v, ventral; r, right; l, left. (A) Transverse section through the thorax of a *Cited2*$^{+/+}$:*INK4a/ARF*$^{-/-}$ embryo shows normal cardiac anatomy. The interatrial septum (ias) separates the right (ra) and left (la) atria. The right (rv) and left (lv) ventricles are separated by a normal interventricular septum (ivs) (B) Corresponding section of a *Cited2*$^{-/-}$:*INK4a/ARF*$^{-/-}$ embryo shows a ventricular septal defect (VSD). (C) Transverse section through the abdomen of a *Cited2*$^{+/+}$:*INK4a/ARF*$^{-/-}$ embryo showing normal right (rad) and left (lad) adrenal glands and left kidney (lk). (D) Corresponding section of a *Cited2*$^{-/-}$:*INK4a/ARF*$^{-/-}$ embryo shows lack of right and left adrenal glands. (E and F) Cranial development in *Cited2*$^{+/+}$:*INK4a/ARF*$^{-/-}$ and *Cited2*$^{-/-}$:*INK4a/ARF*$^{-/-}$ embryos at 14.5 dpc. Scale bar, 1 mm. (E) *Cited2*$^{+/+}$:*INK4a/ARF*$^{-/-}$ embryo showing normal cranial development. (F) *Cited2*$^{-/-}$:*INK4a/ARF*$^{-/-}$ embryo showing exencephaly.

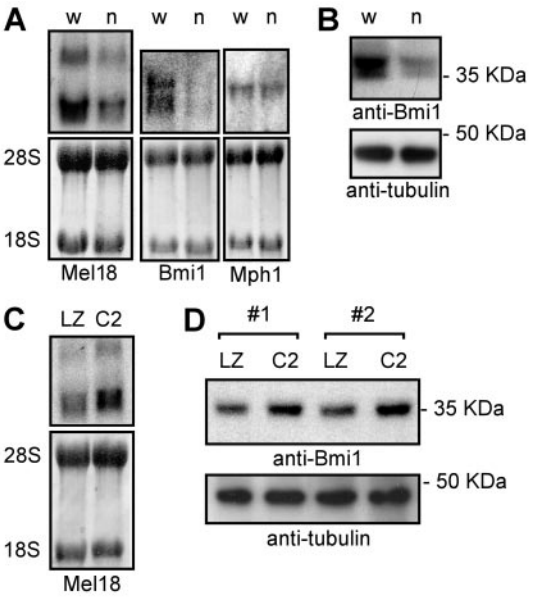

FIG. 7. Expression of *Mel18* and *Bmi1* in fibroblasts lacking *Cited2*. (A) Northern blots of total RNA obtained from *Cited2*$^{+/+}$ (w) and *Cited2*$^{-/-}$ (n) fibroblasts derived from littermate embryos. The top panels show blots probed for Mel18, Bmi1, or Mph1, as indicated. Two Mel18 isoforms are noted (52). The bottom panels show 28S and 18S RNA species to show equal loading. (B) Western blot of total cell lysate probed with an anti-Bmi1 monoclonal antibody (top) and reprobed with an antitubulin monoclonal antibody (bottom) to show equal loading. (C) Northern blot of total RNA obtained from *Cited2*$^{-/-}$ fibroblasts infected in parallel with retroviruses. LZ indicates infection with LZRS (control) retrovirus, and C2 indicates infection with CITED2-expressing retrovirus. The top panel shows a blot probed with a Mel18 cDNA. The bottom panel shows 28S and 18S RNA species to show equal loading. (D) Western blot of total cell lysate from *Cited2*$^{-/-}$ fibroblasts. LZ indicates infection with LZRS (control) retrovirus and C2 indicates infection with CITED2-expressing retrovirus. The experiment was performed in duplicate using independently isolated *Cited2*$^{-/-}$ fibroblast lines (nos. 1 and 2). The top panel shows a blot probed with an anti-Bmi1 antibody. The bottom panel shows a blot probed with an antitubulin antibody to show equal loading.

such as *Ras* (37, 46) and *MEK* (35) in primary cells results in senescence by activating the p19^{ARF}-p53 pathway.

The results presented here provide genetic evidence that *Cited2*, a growth factor and cytokine-inducible gene with oncogenic potential (51), is necessary for fibroblast proliferation in culture. Fibroblasts lacking *Cited2* stop dividing prematurely, display typical senescent morphology, and express senescence-associated β-galactosidase (Fig. 1 and 2). These results suggested that they are hypersensitive to culture-induced stress. The expression of p16^{INK4a}, p19^{ARF}, and p15^{INK4b} but not p19^{INK4d} was markedly increased in *Cited2*$^{-/-}$ fibroblasts (Fig. 3). These results indicated that *Cited2* is required for the coordinated repression of the physically linked *INK4a/ARF* and *INK4b* genes. *INK4a/ARF* and *INK4b* were also repressed by complementation with CITED2, which also enhanced cellular proliferation, suggesting a causal mechanism (Fig. 4). Although the reduction of *INK4a/ARF* and *INK4b* by retrovirally transduced CITED2 was modest, it was reproducible and supports the idea that *Cited2* represses these genes.

Embryos lacking *Cited2* invariably have heart and adrenal gland defects, and ~50% of embryos have exencephaly (9, 42–44). Premature fibroblast senescence occurred regardless of the presence or absence of exencephaly (e.g., the mutant embryos in Fig. 1A and B had normal neural development). Nevertheless, it was possible that the embryonic heart or adrenal malformation itself affects (through secondary changes) the growth of fibroblasts. To address this issue, we performed the complementation experiment with CITED2 and showed, reproducibly, that complementation with retroviral CITED2 markedly enhances proliferation of *Cited2*$^{-/-}$ fibroblasts (Fig. 4A). This effect was specific, as it was not seen with a CITED2 mutant lacking residues 215 to 270. Successful complementation indicates that no secondary change, e.g., one induced by the heart, adrenal, or neural defect, was responsible for the fibroblast growth defect. Thus, the premature senescence observed in fibroblasts lacking *Cited2* is indeed specific and is unlikely to be due to the preexisting embryonic malformation.

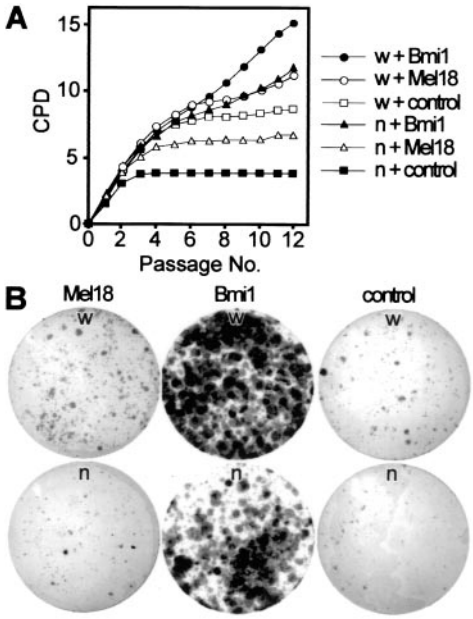

FIG. 8. Growth properties of *Cited2*$^{-/-}$ and *Cited2*$^{+/+}$ embryonic fibroblasts infected with Bmi1- and Mel18-expressing retroviruses. (A) Proliferation of *Cited2*$^{-/-}$ (n) and *Cited2*$^{+/+}$ (w) fibroblasts (derived from littermate embryos on a C57BL/6J background at 13.5 dpc) infected with Bmi1, Mel18, or control retroviruses. Fibroblasts were harvested, infected with retroviruses the following day, replated on day 4 (referred to as P0), and passaged in parallel every 3 days at identical conditions. The proliferation of retrovirally complemented fibroblasts is shown as plots of CPD versus passage number. (B) Colony formation assay. *Cited2*$^{-/-}$ and *Cited2*$^{+/+}$ fibroblasts (at passage 6) infected with the indicated retroviruses were plated at a density of 4,000 cells per 9-cm plate, and colonies were visualized with Giemsa stain after 16 days.

Notably, residues 215 to 270 of CITED2 contain the overlapping TFAP2 and CBP/p300 binding domains (9, 12), suggesting that binding of CITED2 to CBP/p300 and/or TFAP2 is required for enhancement of cell proliferation.

We also found that deletion of *INK4a/ARF* completely rescued the proliferation defect in fibroblasts lacking *Cited2* (Fig. 5). This finding was observed reproducibly in fibroblasts obtained from independently isolated embryos. As the proliferation defect in *Cited2*-deficient fibroblasts is reproducibly observed on both mixed (Fig. 1A and Fig. 5A and C) and pure (Fig. 1B) genetic backgrounds, the reproducible rescue of senescence by deletion of *INK4a/ARF* in *Cited2*$^{-/-}$ fibroblasts indicates that random segregation of genetic modifiers in these experiments does not likely play an important role. Taken together with the increased levels of *INK4a/ARF* observed in *Cited2*$^{-/-}$ fibroblasts and the suppression of *INK4a/ARF* by complementation with CITED2, these experiments show that the elevated levels of *INK4a/ARF* observed in *Cited2*$^{-/-}$ fibroblasts play a major causal role in generating the premature senescence phenotype and that *INK4a/ARF* is a critical downstream target of *Cited2* in fibroblasts. The complete rescue in cell proliferation that we observed also indicates that no other downstream mechanism (e.g., the activation of p53 or p27 by a different mechanism, such as HIF-1 activation in cells lacking *Cited2*) is likely to be involved. These results are also supported by experiments which show that fibroblasts lacking *Cited2* are efficiently immortalized by overexpression of the p19^{ARF} repressor TBX2 (24) and by antisense p19^{ARF} retrovirus (16) (K. R. Kranc and S. Bhattacharya, unpublished observations).

The above data indicated that *Cited2* enhances cell proliferation by repressing *INK4a/ARF*. However, deletion of the *INK4a/ARF* locus did not rescue the embryonic malformations (cardiac, adrenal, and neural) associated with mutation in *Cited2* (Fig. 6). Thus, the *Cited2*-mediated repression of *INK4a/ARF* observed in fibroblasts does not appear to play a significant role in embryonic development. This finding indicates that *Cited2* has two independent functions: first, a role in embryonic development, and second, a role in fibroblast proliferation under conditions of culture-induced stress. One possible mechanism is that *Cited2* positively regulates genes that not only repress *INK4a/ARF* but also have independent roles in development. Members of the polycomb family (e.g., *Bmi1* and *Mel18*) are known to play these dual roles (2, 25, 55).

Genetic evidence indicates that in primary mouse fibroblasts Bmi1 represses p16^{INK4a} and p19^{ARF} and Mel18 represses p16^{INK4a} (25). Deletion of either *Bmi1* or its paralog *Mel18* leads to reduced lymphocyte precursor proliferation and premature proliferation arrest of primary mouse embryonic fibroblasts (3, 25). *Bmi1* is also necessary for self-renewal of hematopoietic stem cells (32, 40). Deletion of *INK4a/ARF* in mice lacking *Bmi1* rescues premature fibroblast senescence and postnatal cerebellar and lymphoid defects (25). However, *Mel18* has more complex functions, as evidenced by the fact that it can also function as a cell proliferation inhibitor in other cell types (29, 53). Differences in Bmi1 and Mel18 function are also suggested by distinct phenotypes observed in mutant mice: for instance, cerebellar defects are observed in mice lacking *Bmi1*, and colonic smooth muscle defects are seen in mice lacking *Mel18* (2, 55). Bmi1 and Mel18 function as transcriptional repressors that interact with a similar set of polycomb-group proteins (6, 20, 22, 26, 54). They function during development to repress *Hox* genes, and deletion of either gene leads to defects in anteroposterior axis formation (2, 55). *Mel18* and *Bmi1* act synergistically in a dose-dependent manner during development to maintain *Hox* gene expression and cell survival (4). Importantly, we have observed anteroposterior patterning defects in *Cited2* mutant embryos. These include fusion of cranial ganglia (9) and of the cervical vertebrae (S. D. Bamforth and S. Bhattacharya, unpublished observations). These observations prompted us to examine *Bmi1* and *Mel18* expression in fibroblasts lacking *Cited2*.

We found that fibroblasts lacking *Cited2* have a marked reduction in levels of Bmi1 and Mel18 transcripts (Fig. 7). Complementation of *Cited2*$^{-/-}$ fibroblasts with CITED2 led to a modest increase in the expression of Bmi1 and Mel18. We also found that both Bmi1 and Mel18 enhanced the proliferation of fibroblasts regardless of the *Cited2* genotype (Fig. 8), indicating that *Cited2* is not necessary for proliferation enhancement by these polycomb-group genes and supporting the idea that *Bmi1* and *Mel18* function downstream of *Cited2*. However, after infection with Bmi1- and Mel18-expressing retroviruses, *Cited2*$^{+/+}$ fibroblasts proliferated faster than *Cited2*$^{-/-}$ fibroblasts, implying that *Cited2* deficiency cannot be completely rescued by overexpression of Bmi1 or Mel18 indi-

vidually. One possibility is that other *Cited2* functions that are independent of Bmi1 or Mel18 may be important. Another possibility is that *Cited2* is required for the coordinated induction of *Bmi1* and *Mel18*, which is not mimicked by the forced expression of either Bmi1 or Mel18 alone.

In summary, these data indicate that *Cited2* is required for normal *Bmi1* and *Mel18* expression in primary mouse embryonic fibroblasts and that *Bmi1* and *Mel18* function downstream of *Cited2*. The mechanism by which *Cited2* induces *Bmi1* and *Mel18* is not understood at present. One possibility is that a coactivation function of Cited2 is required for *Bmi1*/*Mel18* expression. Alternatively, Cited2 may function several steps away, even perhaps via nonautonomous cell mechanisms, to control Bmi1/Mel18 expression. These possibilities require further investigation. Taken together, our results provide genetic evidence that *Cited2* controls the expression of *INK4a*/*ARF* and fibroblast proliferation at least in part via the polycomb-group genes *Bmi1* and *Mel18* and provide a mechanism by which *Cited2* may function as an oncogene.

ACKNOWLEDGMENTS

We thank Ronald DePinho for the generous gift of *INK4a*/*ARF* mutant mice, Charles Sherr and Gordon Peters for gifts of probes, Garry Nolan for LZRS plasmids and Phoenix cells, and Derek Davies (Cancer Research UK) for help with cytometry.

K.R.K. is a Wellcome Prize student and a Keith Murray senior scholar at Lincoln College. These studies were funded by a Wellcome Trust senior fellowship award to S.B.

REFERENCES

1. **Ait-Si-Ali, S., A. Polesskaya, S. Filleur, R. Ferreira, A. Duquet, P. Robin, A. Vervish, D. Trouche, F. Cabon, and A. Harel-Bellan.** 2000. CBP/p300 histone acetyl-transferase activity is important for the G1/S transition. Oncogene **19:**2430–2437.
2. **Akasaka, T., M. Kanno, R. Balling, M. A. Mieza, M. Taniguchi, and H. Koseki.** 1996. A role for *mel-18*, a Polycomb group-related vertebrate gene, during the anteroposterior specification of the axial skeleton. Development **122:**1513–1522.
3. **Akasaka, T., K. Tsuji, H. Kawahira, M. Kanno, K. Harigaya, L. Hu, Y. Ebihara, T. Nakahata, O. Tetsu, M. Taniguchi, and H. Koseki.** 1997. The role of *mel-18*, a mammalian Polycomb group gene, during IL-7-dependent proliferation of lymphocyte precursors. Immunity **7:**135–146.
4. **Akasaka, T., M. van Lohuizen, N. van der Lugt, Y. Mizutani-Koseki, M. Kanno, M. Taniguchi, M. Vidal, M. Alkema, A. Berns, and H. Koseki.** 2001. Mice doubly deficient for the Polycomb Group genes *Mel18* and *Bmi1* reveal synergy and requirement for maintenance but not initiation of Hox gene expression. Development **128:**1587–1597.
5. **Alani, R. M., A. Z. Young, and C. B. Shifflett.** 2001. Id1 regulation of cellular senescence through transcriptional repression of p16/Ink4a. Proc. Natl. Acad. Sci. USA **98:**7812–7816.
6. **Alkema, M. J., M. Bronk, E. Verhoeven, A. Otte, L. J. van't Veer, A. Berns, and M. van Lohuizen.** 1997. Identification of Bmi1-interacting proteins as constituents of a multimeric mammalian polycomb complex. Genes Dev. **11:**226–240.
7. **Ausubel, F., R. Brent, R. E. Kingston, D. D. Moore, J. G. Seidman, J. A. Smith, and K. Struhl.** 1995. Short protocols in molecular biology, 3rd ed. John Wiley & Sons, Inc., New York, N.Y.
8. **Avantaggiati, M. L., V. Ogryzko, K. Gardner, A. Giordano, A. S. Levine, and K. Kelly.** 1997. Recruitment of p300/CBP in p53-dependent signal pathways. Cell **89:**1175–1184.
9. **Bamforth, S. D., J. Braganca, J. J. Eloranta, J. N. Murdoch, F. I. Marques, K. R. Kranc, H. Farza, D. J. Henderson, H. C. Hurst, and S. Bhattacharya.** 2001. Cardiac malformations, adrenal agenesis, neural crest defects and exencephaly in mice lacking Cited2, a new Tfap2 co-activator. Nat. Genet. **29:**469–474.
10. **Barbera, J. P., T. A. Rodriguez, N. D. Greene, W. J. Weninger, A. Simeone, A. J. Copp, R. S. Beddington, and S. Dunwoodie.** 2002. Folic acid prevents exencephaly in Cited2 deficient mice. Hum. Mol. Genet. **11:**283–293.
11. **Baserga, R.** 1989. Measuring parameters of growth, p. 1–16. *In* R. Baserga (ed.), Cell growth and division: a practical approach. Oxford University Press, Oxford, United Kingdom.
12. **Bhattacharya, S., C. L. Michels, M. K. Leung, Z. P. Arany, A. L. Kung, and D. M. Livingston.** 1999. Functional role of p35srj, a novel p300/CBP binding protein, during transactivation by HIF-1. Genes Dev. **13:**64–75.
13. **Blasco, M. A., H. W. Lee, M. P. Hande, E. Samper, P. M. Lansdorp, R. A. DePinho, and C. W. Greider.** 1997. Telomere shortening and tumor formation by mouse cells lacking telomerase RNA. Cell **91:**25–34.
14. **Braganca, J., J. J. Eloranta, S. D. Bamforth, J. C. Ibbitt, H. C. Hurst, and S. Bhattacharya.** 2003. Physical and functional interactions among AP-2 transcription factors, p300/CREB-binding protein, and CITED2. J. Biol. Chem. **278:**16021–16029.
15. **Braganca, J., T. Swingler, F. I. Marques, T. Jones, J. J. Eloranta, H. C. Hurst, T. Shioda, and S. Bhattacharya.** 2002. Human CREB-binding protein/p300-interacting transactivator with ED-rich tail (CITED) 4, a new member of the CITED family, functions as a co-activator for transcription factor AP-2. J. Biol. Chem. **277:**8559–8565.
16. **Carnero, A., J. D. Hudson, C. M. Price, and D. H. Beach.** 2000. p16INK4A and p19ARF act in overlapping pathways in cellular immortalization. Nat. Cell Biol. **2:**148–155.
17. **Dimri, G. P., X. Lee, G. Basile, M. Acosta, G. Scott, C. Roskelley, E. E. Medrano, M. Linskens, I. Rubelj, O. Pereira-Smith, et al.** 1995. A biomarker that identifies senescent human cells in culture and in aging skin in vivo. Proc. Natl. Acad. Sci. USA **92:**9363–9367.
18. **Frank, K. M., N. E. Sharpless, Y. Gao, J. M. Sekiguchi, D. O. Ferguson, C. Zhu, J. P. Manis, J. Horner, R. A. DePinho, and F. W. Alt.** 2000. DNA ligase IV deficiency in mice leads to defective neurogenesis and embryonic lethality via the p53 pathway. Mol. Cell **5:**993–1002.
19. **Goodman, R. H., and S. Smolik.** 2000. CBP/p300 in cell growth, transformation, and development. Genes Dev. **14:**1553–1577.
20. **Gunster, M. J., D. P. Satijn, K. M. Hamer, J. L. den Blaauwen, D. de Bruijn, M. J. Alkema, M. van Lohuizen, R. van Driel, and A. P. Otte.** 1997. Identification and characterization of interactions between the vertebrate polycomb-group protein BMI1 and human homologs of polyhomeotic. Mol. Cell. Biol. **17:**2326–2335.
21. **Hannon, G. J., and D. Beach.** 1994. p15INK4B is a potential effector of TGF-beta-induced cell cycle arrest. Nature **371:**257–261.
22. **Hashimoto, N., H. W. Brock, M. Nomura, M. Kyba, J. Hodgson, Y. Fujita, Y. Takihara, K. Shimada, and T. Higashinakagawa.** 1998. RAE28, BMI1, and M33 are members of heterogeneous multimeric mammalian Polycomb group complexes. Biochem. Biophys. Res. Commun. **245:**356–365.
23. **Hirai, H., M. F. Roussel, J. Y. Kato, R. A. Ashmun, and C. J. Sherr.** 1995. Novel INK4 proteins, p19 and p18, are specific inhibitors of the cyclin D-dependent kinases CDK4 and CDK6. Mol. Cell. Biol. **15:**2672–2681.
24. **Jacobs, J. J., P. Keblusek, E. Robanus-Maandag, P. Kristel, M. Lingbeek, P. M. Nederlof, T. van Welsem, M. J. van De Vijver, E. Y. Koh, G. Q. Daley, and M. van Lohuizen.** 2000. Senescence bypass screen identifies *TBX2*, which represses *Cdkn2a* (*p19^{ARF}*) and is amplified in a subset of human breast cancers. Nat. Genet. **26:**291–299.
25. **Jacobs, J. J., K. Kieboom, S. Marino, R. A. DePinho, and M. van Lohuizen.** 1999. The oncogene and Polycomb-group gene *bmi-1* regulates cell proliferation and senescence through the *ink4a* locus. Nature **397:**164–168.
26. **Jacobs, J. J., and M. van Lohuizen.** 1999. Cellular memory of transcriptional states by Polycomb-group proteins. Semin. Cell Dev. Biol. **10:**227–235.
27. **Kamijo, T., E. van de Kamp, M. J. Chong, F. Zindy, J. A. Diehl, C. J. Sherr, and P. J. McKinnon.** 1999. Loss of the ARF tumor suppressor reverses premature replicative arrest but not radiation hypersensitivity arising from disabled Atm function. Cancer Res. **59:**2464–2469.
28. **Kamijo, T., F. Zindy, M. F. Roussel, D. E. Quelle, J. R. Downing, R. A. Ashmun, G. Grosveld, and C. J. Sherr.** 1997. Tumor suppression at the mouse INK4a locus mediated by the alternative reading frame product p19ARF. Cell **91:**649–659.
29. **Kanno, M., M. Hasegawa, A. Ishida, K. Isono, and M. Taniguchi.** 1995. mel-18, a Polycomb group-related mammalian gene, encodes a transcriptional negative regulator with tumor suppressive activity. EMBO J. **14:**5672–5678.
30. **Krimpenfort, P., K. C. Quon, W. J. Mooi, A. Loonstra, and A. Berns.** 2001. Loss of p16Ink4a confers susceptibility to metastatic melanoma in mice. Nature **413:**83–86.
31. **Kung, A. L., V. I. Rebel, R. T. Bronson, L. E. Ch'ng, C. A. Sieff, D. M. Livingston, and T. P. Yao.** 2000. Gene dose-dependent control of hematopoiesis and hematologic tumor suppression by CBP. Genes Dev. **14:**272–277.
32. **Lessard, J., and G. Sauvageau.** 2003. Bmi-1 determines the proliferative capacity of normal and leukaemic stem cells. Nature **423:**255–260.
33. **Leung, M. K., T. Jones, C. L. Michels, D. M. Livingston, and S. Bhattacharya.** 1999. Molecular cloning and chromosomal localization of the human CITED2 gene encoding p35srj/Mrg1. Genomics **61:**307–313.
34. **Lill, N. L., S. R. Grossman, D. Ginsberg, J. DeCaprio, and D. M. Livingston.** 1997. Binding and modulation of p53 by p300/CBP coactivators. Nature **387:**823–827.
35. **Lin, A. W., M. Barradas, J. C. Stone, L. van Aelst, M. Serrano, and S. W. Lowe.** 1998. Premature senescence involving p53 and p16 is activated in response to constitutive MEK/MAPK mitogenic signaling. Genes Dev. **12:**3008–3019.
36. **Loo, D., C. Rawson, T. Ernst, S. Shirahata, and D. Barnes.** 1989. Primary

and multipassage culture of mouse embryo cells in serum-containing and serum-free media, p. 17–35. *In* R. Baserga (ed.), Cell growth and division: a practical approach. Oxford University Press, Oxford, United Kingdom.
37. **Malumbres, M., I. Perez De Castro, M. I. Hernandez, M. Jimenez, T. Corral, and A. Pellicer.** 2000. Cellular response to oncogenic Ras involves induction of the Cdk4 and Cdk6 inhibitor p15^{INK4b}. Mol. Cell. Biol. **20:**2915–2925.
38. **Miller, R. W., and J. H. Rubinstein.** 1995. Tumors in Rubinstein-Taybi syndrome. Am. J. Med. Genet. **56:**112–115.
39. **Oike, Y., N. Takakura, A. Hata, T. Kaname, M. Akizuki, Y. Yamaguchi, H. Yasue, K. Araki, K. Yamamura, and T. Suda.** 1999. Mice homozygous for a truncated form of CREB-binding protein exhibit defects in hematopoiesis and vasculo-angiogenesis. Blood **93:**2771–2779.
40. **Park, I. K., D. Qian, M. Kiel, M. W. Becker, M. Pihalja, I. L. Weissman, S. J. Morrison, and M. F. Clarke.** 2003. Bmi-1 is required for maintenance of adult self-renewing haematopoietic stem cells. Nature **423:**302–305.
41. **Petrij, F., R. H. Giles, H. G. Dauwerse, J. J. Saris, R. C. M. Hennekam, M. Masuno, N. Tommerup, G. B. Ommen, R. H. Goodman, D. J. M. Peters, and M. H. Breuning.** 1995. Rubinstein-Taybi syndrome caused by mutations in the transcriptional co-activator CBP. Nature **376:**348–351.
42. **Schneider, J. E., S. D. Bamforth, C. R. Farthing, K. Clarke, S. Neubauer, and S. Bhattacharya.** 2003. High-resolution imaging of normal anatomy, and neural and adrenal malformations in mouse embryos using magnetic resonance microscopy. J. Anat. **202:**239–247.
43. **Schneider, J. E., S. D. Bamforth, C. R. Farthing, K. Clarke, S. Neubauer, and S. Bhattacharya.** 2003. Rapid identification and 3D reconstruction of complex cardiac malformations in transgenic mouse embryos using fast gradient echo sequence magnetic resonance imaging. J. Mol. Cell. Cardiol. **35:**217–222.
44. **Schneider, J. E., S. D. Bamforth, S. M. Grieve, K. Clarke, S. Bhattacharya, and S. Neubauer.** 2003. High-resolution, high-throughput magnetic resonance imaging of mouse embryonic anatomy using a fast gradient-echo sequence. MAGMA **16:**43–51.
45. **Serrano, M., H. Lee, L. Chin, C. Cordon-Cardo, D. Beach, and R. A. DePinho.** 1996. Role of the INK4a locus in tumor suppression and cell mortality. Cell **85:**27–37.
46. **Serrano, M., A. W. Lin, M. E. McCurrach, D. Beach, and S. W. Lowe.** 1997. Oncogenic ras provokes premature cell senescence associated with accumulation of p53 and p16^{INK4a}. Cell **88:**593–602.
47. **Sharpless, N. E., N. Bardeesy, K. H. Lee, D. Carrasco, D. H. Castrillon, A. J. Aguirre, E. A. Wu, J. W. Horner, and R. A. DePinho.** 2001. Loss of p16Ink4a with retention of p19Arf predisposes mice to tumorigenesis. Nature **413:**86–91.
48. **Sherr, C. J., and R. A. DePinho.** 2000. Cellular senescence: mitotic clock or culture shock? Cell **102:**407–410.
49. **Sherr, C. J., and J. D. Weber.** 2000. The ARF/p53 pathway. Curr. Opin. Genet. Dev. **10:**94–99.
50. **Shikama, N., J. Lyon, and N. B. La Thangue.** 1997. The p300/CBP family: integrating signals with transcription factors and chromatin. Trends Cell. Biol. **7:**230–236.
51. **Sun, H. B., Y. X. Zhu, T. Yin, G. Sledge, and Y. C. Yang.** 1998. MRG1, the product of a melanocyte-specific gene related gene, is a cytokine-inducible transcription factor with transformation activity. Proc. Natl. Acad. Sci. USA **95:**13555–13560.
52. **Tagawa, M., T. Sakamoto, K. Shigemoto, H. Matsubara, Y. Tamura, T. Ito, I. Nakamura, A. Okitsu, K. Imai, and M. Taniguchi.** 1990. Expression of novel DNA-binding protein with zinc finger structure in various tumor cells. J. Biol. Chem. **265:**20021–20026.
53. **Tetsu, O., H. Ishihara, R. Kanno, M. Kamiyasu, H. Inoue, T. Tokuhisa, M. Taniguchi, and M. Kanno.** 1998. mel-18 negatively regulates cell cycle progression upon B cell antigen receptor stimulation through a cascade leading to c-myc/cdc25. Immunity **9:**439–448.
54. **Trimarchi, J. M., B. Fairchild, J. Wen, and J. A. Lees.** 2001. The E2F6 transcription factor is a component of the mammalian Bmi1-containing polycomb complex. Proc. Natl. Acad. Sci. USA **98:**1519–1524.
55. **van der Lugt, N. M., J. Domen, K. Linders, M. van Roon, E. Robanus-Maandag, H. te Riele, M. van der Valk, J. Deschamps, M. Sofroniew, M. van Lohuizen, et al.** 1994. Posterior transformation, neurological abnormalities, and severe hematopoietic defects in mice with a targeted deletion of the bmi-1 proto-oncogene. Genes Dev. **8:**757–769.
56. **Weitzman, J. B., L. Fiette, K. Matsuo, and M. Yaniv.** 2000. JunD protects cells from p53-dependent senescence and apoptosis. Mol. Cell **6:**1109–1119.
57. **Weninger, W. J., and T. Mohun.** 2002. Phenotyping transgenic embryos: a rapid 3-D screening method based on episcopic fluorescence image capturing. Nat. Genet. **30:**59–65.
58. **Yahata, T., M. P. de Caestecker, R. J. Lechleider, S. Andriole, A. B. Roberts, K. J. Isselbacher, and T. Shioda.** 2000. The MSG1 non-DNA-binding transactivator binds to the p300/CBP coactivators, enhancing their functional link to the Smad transcription factors. J. Biol. Chem. **275:**8825–8834.
59. **Yahata, T., H. Takedatsu, S. L. Dunwoodie, J. Braganca, T. Swingler, S. L. Withington, J. Hur, K. R. Coser, K. J. Isselbacher, S. Bhattacharya, and T. Shioda.** 2002. Cloning of mouse Cited4, a member of the CITED family p300/CBP-binding transcriptional coactivators: induced expression in mammary epithelial cells. Genomics **80:**601–613.
60. **Yao, T. P., S. P. Oh, M. Fuchs, N. D. Zhou, L. E. Ch'ng, D. Newsome, R. T. Bronson, E. Li, D. M. Livingston, and R. Eckner.** 1998. Gene dosage-dependent embryonic development and proliferation defects in mice lacking the transcriptional integrator p300. Cell **93:**361–372.
61. **Yin, Z., J. Haynie, X. Yang, B. Han, S. Kiatchoosakun, J. Restivo, S. Yuan, N. R. Prabhakar, K. Herrup, R. A. Conlon, B. D. Hoit, M. Watanabe, and Y. C. Yang.** 2002. The essential role of Cited2, a negative regulator for HIF-1α, in heart development and neurulation. Proc. Natl. Acad. Sci. USA **99:**10488–10493.
62. **Zindy, F., D. E. Quelle, M. F. Roussel, and C. J. Sherr.** 1997. Expression of the p16INK4a tumor suppressor versus other INK4 family members during mouse development and aging. Oncogene **15:**203–211.